

Biconical Antennas with Unequal Cone Angles

Surendra N. Samaddar, *Life Senior Member, IEEE*, and Eric L. Mokole, *Member, IEEE*

Abstract—The problem of radiation and reception of electromagnetic waves associated with a spherically capped biconical antenna having unequal cone angles ψ_1 and ψ_2 is investigated. Both cones that comprise a bicone are excited symmetrically at the apices so that the only higher order modes are TM. A variational expression for the terminal admittance is derived. Under the wide-angle approximation, expressions for the radiated field, the effective height, and the terminal admittance are obtained. In addition, limiting values of these quantities are derived for electrically small and electrically large wide-angle bicones. The results for arbitrary cone angles are new and subsume results that appear in the existing literature as special cases such as where $\psi_1 = \psi_2$ or $\psi_2 = \pi/2$. Moreover, the approximations of this paper are more accurate than many in the literature. It is argued that the radiation pattern of an electrically small cone is proportional to $\sin \theta$, which is similar to that of a short dipole; whereas the pattern behaves like $1/\sin \theta$ for electrically large cones. The parameter θ is the angle from the bicone's axis of symmetry to the observation direction. Consequently, the direction of maximum radiation changes with exciting frequency for a bicone of fixed length. Although most of the analyses are presented in the frequency-domain, time-domain responses of bicones are discussed for some special cases that are similar to situations considered by Harrison and Williams. In particular, the time-domain radiated field and the received voltage are shown to depend on the input's passband and on the match between the source and the bicone.

I. INTRODUCTION

IN this paper, the biconical antenna analyses provided by Schelkunoff [1], Smith [2], Tai [3]–[5], Papas and King [6], [7], and Sandler and King [8] are generalized by considering axially symmetric bicones having unequal cone angles. The geometry of the antenna configuration is shown in Fig. 1, and (r, θ, ϕ) are spherical coordinates. The common axis of the two cones is oriented along the z axis and the cone angles ψ_1 and ψ_2 satisfy $0 < \psi_1 < \pi/2$ and $0 < \psi_2 \leq \pi - \psi_1$. Relative to θ , the lateral surfaces of the upper and lower cones correspond to $\theta = \psi_1$ and $\theta = \pi - \psi_2$, respectively. By a proper choice of ψ_1 and ψ_2 , the exit aperture of the antenna can be adjusted so that the radiated power will be directed in a desired direction, which is one of the motivations behind this investigation. Furthermore, knowledge of biconical antenna characteristics is helpful in understanding why TEM horns, V-antennas, triangular plates, and bow-tie antennas are very wide band.

The cones are excited symmetrically at the apices so that only TEM and TM modes are generated. The field components can then be expressed in terms of a scalar

Manuscript received October 10, 1996; revised September 25, 1997. This work was supported by the Naval Research Laboratory and the Office of Naval Research.

The authors are with Naval Research Laboratory, Washington, DC 20375 USA.

Publisher Item Identifier S 0018-926X(98)01486-0.

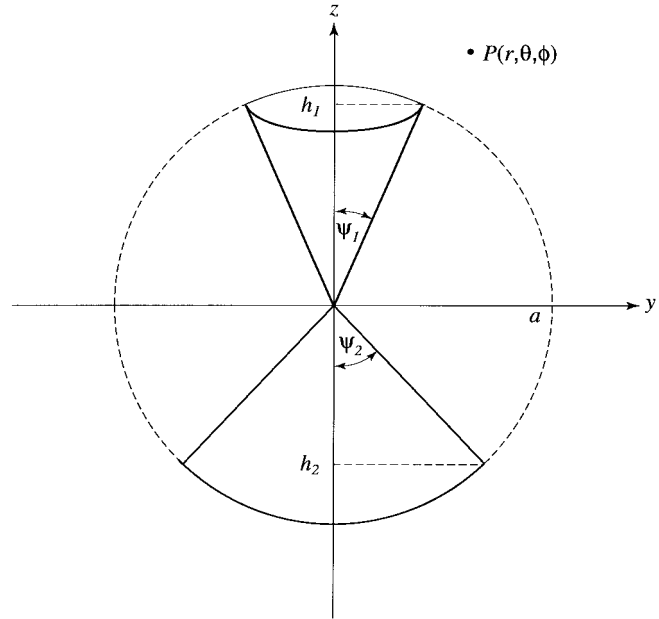


Fig. 1. Cross-sectional view of spherically capped biconical antenna with equal slant heights denoted by a and with unequal cone angles ψ_1 and ψ_2 in rectangular (x, y, z) and spherical (r, θ, ϕ) coordinates. The x axis points out of the paper and the angle ϕ about the z axis is measured from the x axis toward the y axis. The dotted curve represents a sphere of radius a and the lengths h_1 and h_2 are the altitudes of the top cone and bottom cone, respectively.

function $\Pi(r, \theta)$ [1]–[5], which is equivalent to the radial component of the vector potential and is azimuthally invariant. Formal expressions for the field components are presented first in each of the regions $0 \leq r \leq a$ and $r \geq a$, where a is the length of each cone and corresponds to the radius of the sphere in Fig. 1. On using these field components, a variational expression for the terminal admittance is derived in Sections II-A and II-B. When $\psi_1 = \psi_2$, this variational expression agrees with Tai's result [5].

Also of interest are the wide-band and ultrawide-band behaviors of biconical antennas, which have application in surveillance and communications. Papas and King [6] demonstrated that both the input resistance and reactance of wide-angle bicones having cone angles exceeding 40° are very slowly varying functions of frequency for very wide frequency ranges. Furthermore, they showed that the higher-order TM modes in the antenna region ($0 \leq r \leq a$) can be neglected for wide-angle bicones. Under this wide-angle approximation, general results for a bicone's effective length, input impedance, terminal admittance, and radiated field are derived (Section II-C). These results are further analyzed for the limiting cases of electrically small and large wide-angle cones. Radiation patterns for two specific wide-angle bicones with $a = 20$

inches are discussed to contrast the behavior of equal cone angles versus that of unequal cone angles: 1) $\psi_1 = \psi_2 = 53.1^\circ$ and 2) $\psi_1 = 53.1^\circ$ and $\psi_2 = 70^\circ$. In Section III, the transient responses of wide-angle biconical antennas for some special cases, similar to the situations considered by Harrison and Williams [9], are studied.

II. ANALYSIS

In this section, formal expressions of the electric- and magnetic-field components for the antenna region ($0 \leq r \leq a$) and its complement ($r > a$) are expanded in terms of series involving Bessel (J_ν), Legendre (P_ν), and Hankel ($H_\nu^{(2)}$) functions. The unknown coefficients of these expansions and the terminal admittance Y_t of the bicone at $r = a$ are determined. The expression for Y_t is recast in a variational form, which is evaluated to obtain a series representation of Y_t . At this point, the expressions for the fields, the input impedance Z_{in} , the effective height h_e , and Y_t are simplified by using a wide-angle approximation for the cones. These results are reduced further by applying approximations for two special cases: electrically small ($ka \ll 1$) and electrically large ($ka \gg 1$) wide-angle cones.

Within the antenna region ($0 < r < a$ and $\psi_1 < \theta < \pi - \psi_2$), the components of the electric and magnetic fields are given by

$$i\omega\epsilon_0 r^2 E_r = - \sum_{\nu_p} \frac{a_{\nu_p}}{2\pi} \frac{S_{\nu_p}(kr)}{S_{\nu_p}(ka)} T_{\nu_p}(\theta) \quad (1a)$$

$$rE_\theta = \frac{I_0 Z_0}{2\pi \sin \theta} [(1 + Z_c Y_t) e^{-ik(r-a)} + (1 - Z_c Y_t) e^{ik(r-a)}] - iZ_0 \sum_{\nu_p} \frac{a_{\nu_p}}{2\pi \nu_p (\nu_p + 1)} \frac{S'_{\nu_p}(kr)}{S_{\nu_p}(ka)} \frac{\partial}{\partial \theta} T_{\nu_p}(\theta) \quad (1b)$$

$$rH_\phi = \frac{I_0}{2\pi \sin \theta} [(1 + Z_c Y_t) e^{-ik(r-a)} - (1 - Z_c Y_t) e^{ik(r-a)}] - \sum_{\nu_p} \frac{a_{\nu_p}}{2\pi \nu_p (\nu_p + 1)} \frac{S_{\nu_p}(kr)}{S_{\nu_p}(ka)} \frac{\partial}{\partial \theta} T_{\nu_p}(\theta) \quad (1c)$$

where S'_{ν_p} denotes differentiation of S_{ν_p} with respect to its argument and $\{a_{\nu_p}\}$ and I_0 are constants that must be determined. Furthermore, by [1], $Z_0 = \sqrt{\mu_0/\epsilon_0} = 120\pi$

$$Z_c(\psi_1, \psi_2) = \frac{Z_0}{2\pi} \int_{\psi_1}^{\pi-\psi_2} \frac{1}{\sin \theta} d\theta = \frac{Z_0}{2\pi} \ln [\cot(\psi_1/2) \cot(\psi_2/2)] \quad (2a)$$

$$T_{\nu_p}(\theta) = P_{\nu_p}(\cos \theta) P_{\nu_p}(-\cos \psi_1) - P_{\nu_p}(-\cos \theta) P_{\nu_p}(\cos \psi_1), \quad (2b)$$

$$S_{\nu_p}(kr) = \sqrt{kr} J_{\nu_p + \frac{1}{2}}(kr), \quad (2c)$$

Equation (2b) satisfies the boundary condition that E_r vanishes on the surface of the bicone for $0 < r < a$: $T_{\nu_p}(\psi_1) = 0$ and $T_{\nu_p}(\pi - \psi_2) = 0$. In general, the index ν_p runs over a countable number of noninteger values, which are determined

by solving the transcendental equation $T_{\nu_p}(\pi - \psi_2) = 0$ for each $p = 1, 2, \dots$. Moreover, taking the limit as r approaches a in (1b) yields

$$I_0(\psi_1, \psi_2) = \frac{a}{2Z_c(\psi_1, \psi_2)} \int_{\psi_1}^{\pi-\psi_2} E_\theta(a, \theta) d\theta. \quad (3)$$

Outside the antenna region ($r > a$)

$$i\omega\epsilon_0 r^2 E_r = - \sum_{l=1}^{\infty} \frac{b_l}{2\pi} \frac{R_l(kr)}{R_l(ka)} P_l(\cos \theta) \quad (4a)$$

$$rE_\theta = -iZ_0 \sum_{l=1}^{\infty} \frac{b_l}{2\pi l(l+1)} \frac{R'_l(kr)}{R_l(ka)} \frac{\partial}{\partial \theta} P_l(\cos \theta) \quad (4b)$$

$$rH_\phi = - \sum_{l=1}^{\infty} \frac{b_l}{2\pi l(l+1)} \frac{R_l(kr)}{R_l(ka)} \frac{\partial}{\partial \theta} P_l(\cos \theta) \quad (4c)$$

where R'_l is the derivative of R_l with respect to its argument, $\{b_l\}$ are unknown constants, and

$$R_l(kr) = \sqrt{kr} H_{l+\frac{1}{2}}^{(2)}(kr). \quad (4d)$$

A. Determination of a_{ν_p} , b_l , and Y_t

Representations for the unknown coefficients a_{ν_p} and b_l and the terminal admittance Y_t of (1) and (4) are determined by applying the continuity conditions at $r = a$ and the orthogonality relations for T_{ν_p} and P_l . In particular, since E_r and rH_ϕ are continuous at $r = a$ for $\psi_1 < \theta < \pi - \psi_2$

$$\sum_{l=1}^{\infty} b_l P_l(\cos \theta) = \sum_{\nu_p} a_{\nu_p} T_{\nu_p}(\theta), \quad \psi_1 < \theta < \pi - \psi_2 \quad (5)$$

$$\frac{2I_0 Z_c Y_t}{\sin \theta} - \sum_{\nu_p} \frac{a_{\nu_p}}{\nu_p (\nu_p + 1)} \frac{\partial}{\partial \theta} T_{\nu_p}(\theta) = - \sum_{l=1}^{\infty} \frac{b_l}{l(l+1)} \frac{\partial}{\partial \theta} P_l(\cos \theta). \quad (6)$$

The manipulations in the remainder of this section simplify the coupling among the unknowns and completely uncouples them under the wide-angle cone assumption, so that each unknown is expressed in terms of known quantities.

Integrating both sides of (6) with respect to θ from ψ_1 to $\pi - \psi_2$ and applying the boundary conditions yield

$$Y_t = \left(\frac{Z_0}{2\pi Z_c} \right)^2 \sum_{l=1}^{\infty} \frac{\hat{b}_l}{l(l+1)} g_l(\mu_1, \mu_2) \quad (7a)$$

where $\mu_1 = \cos \psi_1$, $\mu_2 = \cos \psi_2$

$$\hat{b}_l = \frac{b_l \pi}{Z_0 I_0}$$

and

$$g_l(\mu_1, \mu_2) = P_l(\cos \psi_1) - (-1)^l P_l(\cos \psi_2). \quad (7b)$$

When $\psi_1 = \psi_2 = \psi$, (7a) reduces to

$$Y_t = \left(\frac{Z_0}{2\pi Z_c} \right)^2 \sum_{l=1,3,5,\dots} \frac{2\hat{b}_l}{l} P_l(\cos \psi) \quad (7c)$$

which is (14) of [3].

Setting (1b) and (4b) equal at $r = a$ leads to

$$-\frac{iZ_0}{2\pi a} \sum_{l=1}^{\infty} \frac{b_l M_l}{l(l+1)} \frac{\partial}{\partial \theta} P_l(\cos \theta) = \begin{cases} E_a(\theta), & \psi_1 \leq \theta \leq \pi - \psi_2 \\ 0, & 0 \leq \theta \leq \psi_1 \text{ and } \pi - \psi_2 \leq \theta \leq \pi \end{cases} \quad (8a)$$

where

$$E_a(\theta) \equiv E_\theta(a, \theta) = \frac{I_0 Z_0}{\pi a \sin \theta} - \frac{iZ_0}{2\pi a} \sum_{\nu_p} \frac{a_{\nu_p} N_{\nu_p}}{\nu_p(\nu_p + 1)} \frac{\partial}{\partial \theta} T_{\nu_p}(\theta) \quad (8b)$$

$$M_l = \frac{R'_l(ka)}{R_l(ka)} \quad \text{and} \quad N_{\nu_p} = \frac{S'_{\nu_p}(ka)}{S_{\nu_p}(ka)}. \quad (8c)$$

Multiplying (8a) by $\sin \theta \frac{\partial}{\partial \theta} P_r(\cos \theta)$ for positive integer r , integrating from $\theta = 0$ to $\theta = \pi$, and noting that E_θ vanishes on the spherical caps of the metallic bicone yield

$$g_r(\mu_1, \mu_2) = -iZ_0 \sum_{\nu_p} \frac{a_{\nu_p} r(r+1) N_{\nu_p}}{2\pi \nu_p(\nu_p + 1)} I_{\nu_p, r} + \frac{iZ_0 \hat{b}_r M_r}{\pi(2r+1)\Omega(\psi_2)} \quad (9)$$

where $\mu = \cos \theta$ (see (10a) at the bottom of the page) and

$$\Omega(\psi_2) = 1 + \delta_{\psi_2, \frac{\pi}{2}} = \begin{cases} 1, & \psi_2 \neq \pi/2 \\ 2, & \psi_2 = \pi/2. \end{cases} \quad (10b)$$

The function $\Omega(\psi_2)$ is introduced to account for the situation when the cone with angle ψ_2 is replaced with an infinite perfect conductor at the plane $z = 0$ (Fig. 2) that occurs in [6]–[9]. After applying the orthogonality of $T_{\nu_p}(\theta)$ on $\psi_1 \leq \theta \leq \pi - \psi_2$ to (5), one obtains

$$a_{\nu_p} = \sum_{l=1}^{\infty} b_l \frac{I_{\nu_p, l}}{\hat{I}_{\nu_p, \nu_p}}. \quad (11a)$$

The quantity \hat{I}_{ν_p, ν_p} is given by

$$\hat{I}_{\nu_p, \nu_p} = \int_{-\mu_2}^{\mu_1} [T_{\nu_p}(\mu)]^2 d\mu = \frac{1}{2\nu_p + 1} \left[(1 - \mu_1^2) \frac{\partial}{\partial \nu_p} T_{\nu_p}(\mu_1) \frac{\partial}{\partial \mu} T_{\nu_p}(\mu_1) - (1 - \mu_2^2) \frac{\partial}{\partial \nu_p} T_{\nu_p}(-\mu_2) \frac{\partial}{\partial \mu} T_{\nu_p}(-\mu_2) \right]. \quad (11b)$$

Next, substituting (7b) for \hat{b}_r and (11a) for a_{ν_p} in (9) results in

$$g_r(\mu_1, \mu_2) = \frac{i\hat{b}_r M_r}{\Omega(\psi_2) I_0 (2r+1)} - \frac{ir(r+1)}{2I_0} \sum_{\nu_p} \sum_{l=1}^{\infty} \frac{N_{\nu_p} b_l I_{\nu_p, r} I_{\nu_p, l}}{\nu_p(\nu_p + 1) \hat{I}_{\nu_p, \nu_p}} \quad (12)$$

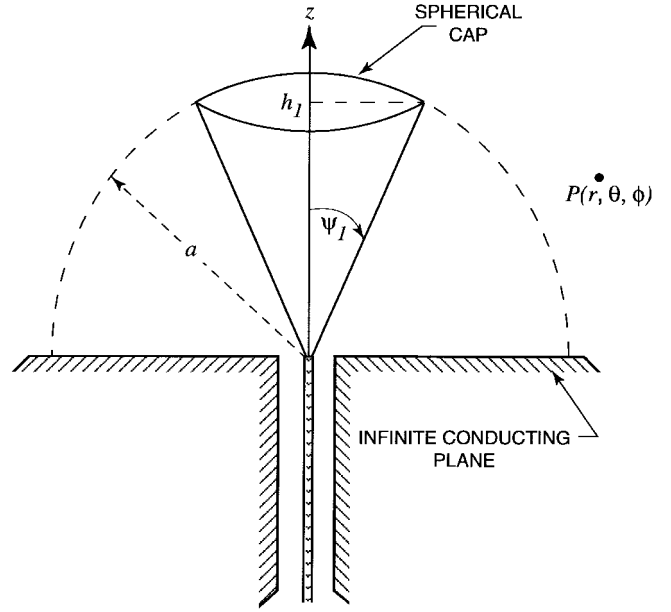


Fig. 2. Cross-sectional view of spherically capped conical antenna in rectangular (x, y, z) and spherical (r, θ, ϕ) coordinates above an infinite conducting ground plane $(xy\text{-plane})$. The cone angle is ψ_1 , the altitude is h_I , and a is both the cone's slant height and the hemisphere's radius. The hemisphere is indicated by the dotted curve.

which involves only the unknowns $\{b_l\}$. Finally, replacement of $g_r(\psi_1, \psi_2)$ in (7a) by the right side of (12) provides an expression for the terminal admittance Y_t

$$Y_t = \frac{iZ_0}{4\pi I_0^2 Z_c^2} \left[\sum_{r=1}^{\infty} \frac{b_r^2 M_r}{\Omega(\psi_2) r(r+1)(2r+1)} - \sum_{\nu_p} \sum_{r=1}^{\infty} \sum_{l=1}^{\infty} \frac{b_r b_l N_{\nu_p}}{2\nu_p(\nu_p + 1)} \frac{I_{\nu_p, r} I_{\nu_p, l}}{\hat{I}_{\nu_p, \nu_p}} \right] \quad (13)$$

in terms of $\{b_l\}$ only. Hence, (11a), (12), and (13) represent the coupling among a_{ν_p} and b_l more simply than (5) and (6).

As mentioned in the introduction, when TM waves or complementary waves in the antenna region are negligible a_{ν_p} can be neglected, which is accurate for wide-angle cones according to [2] and [6]. Letting $a_{\nu_p} = 0$ in (9) implies the following approximate value of \hat{b}_r :

$$\hat{b}_r \simeq -\frac{i\pi(2r+1)}{Z_0 M_r} g_r(\mu_1, \mu_2) \Omega(\psi_2). \quad (14)$$

Subject to the wide-angle cone condition ($a_{\nu_p} \simeq 0$), which may be called the zero-order approximation, the expression for the terminal admittance becomes

$$Y_{t0} = -\frac{iZ_0}{4\pi Z_c^2(\psi_1, \psi_2)} \sum_{r=1}^{\infty} \frac{(2r+1)\Omega(\psi_2)}{r(r+1)M_r} g_r^2(\mu_1, \mu_2). \quad (15)$$

$$I_{\nu_p, r} = \int_{-\mu_2}^{\mu_1} T_{\nu_p}(\mu) P_r(\mu) d\mu = \frac{(1 - \mu_1^2) P_r(\mu_1) \frac{\partial}{\partial \mu} T_{\nu_p}(\mu_1) - (-1)^r (1 - \mu_2^2) P_r(\mu_2) \frac{\partial}{\partial \mu} T_{\nu_p}(-\mu_2)}{r(r+1) - \nu_p(\nu_p + 1)} \quad (10a)$$

Equation (15) can also be obtained from (13) by neglecting the term consisting of the triple sum and then replacing \hat{b}_r with (7b) and (14).

B. Evaluation of Y_t

The representation of Y_t is first recast in terms of the unknown aperture field E_a , which is then expanded in a series involving the sequence $\{T_{\nu_p}\}$. Finally, Y_t is derived by requiring that E_a give a stationary value of Y_t .

With the aid of (8a) and (8b), express b_r and a_{ν_p} as follows in terms of the aperture field $E_a(\theta)$ at $r = a$:

$$b_r = \frac{i2\pi a \Omega(\psi_2)}{Z_0 M_r I_{r,r}} \int_{\psi_1}^{\pi-\psi_2} E_a(\theta) \sin \theta \frac{\partial}{\partial \theta} P_r(\cos \theta) d\theta \quad (16a)$$

$$a_{\nu_p} = \frac{i2\pi a}{Z_0 N_{\nu_p} \hat{I}_{\nu_p, \nu_p}} \int_{\psi_1}^{\pi-\psi_2} E_a(\theta) \sin \theta \frac{\partial}{\partial \theta} T_{\nu_p}(\theta) d\theta \quad (16b)$$

$$I_{r,r} = \int_0^\pi [P_r(\cos \theta)]^2 \sin \theta d\theta = \frac{2}{2r+1}. \quad (16c)$$

Substituting (3), (16a), and (16b) for I_0 , b_r , and a_{ν_p} , respectively, into (6) leads to

$$\begin{aligned} \frac{Y_t}{2\pi \sin \theta} \int_{\psi_1}^{\pi-\psi_2} E_a(\theta') d\theta' - \frac{i}{Z_0} \sum_{\nu_p} \frac{\frac{\partial}{\partial \theta} T_{\nu_p}(\theta)}{\nu_p(\nu_p+1)N_{\nu_p} \hat{I}_{\nu_p, \nu_p}} \\ \times \int_{\psi_1}^{\pi-\psi_2} E_a(\theta') \sin \theta' \frac{\partial}{\partial \theta'} T_{\nu_p}(\theta') d\theta' \\ = -\frac{i}{Z_0} \sum_{r=1}^{\infty} \frac{\Omega(\psi_2) \frac{\partial}{\partial \theta} P_r(\cos \theta)}{r(r+1)M_r I_{r,r}} \\ \times \int_{\psi_1}^{\pi-\psi_2} E_a(\theta') \sin \theta' \frac{\partial}{\partial \theta'} P_r(\cos \theta') d\theta' \end{aligned} \quad (17)$$

the integral equation for the unknown aperture field $E_a(\theta)$. Next, multiply both sides of (17) by $E_a(\theta) \sin \theta$ and integrate with respect to θ from $\theta = \psi_1$ to $\theta = \pi - \psi_2$ to get

$$\begin{aligned} Y_t = \frac{i2\pi}{Z_0} \left[\int_{\psi_1}^{\pi-\psi_2} E_a(\theta) d\theta \right]^{-2} \\ \times \left[\sum_{\nu_p} (\nu_p(\nu_p+1)N_{\nu_p} \hat{I}_{\nu_p, \nu_p})^{-1} \right. \\ \times \left\{ \int_{\psi_1}^{\pi-\psi_2} E_a(\theta) \sin \theta \frac{\partial}{\partial \theta} T_{\nu_p}(\theta) d\theta \right\}^2 \\ - \sum_{r=1}^{\infty} \Omega(\psi_2) (r(r+1)M_r I_{r,r})^{-1} \\ \times \left\{ \int_{\psi_1}^{\pi-\psi_2} E_a(\theta) \sin \theta \frac{\partial}{\partial \theta} P_r(\cos \theta) d\theta \right\}^2 \left. \right]. \end{aligned} \quad (18)$$

It can be shown that the functional Y_t of (18) is in variational form with respect to $E_a(\theta)$; that is, E_a makes Y_t stationary. In other words, the first variation of Y_t is zero for all admissible variations of E_a .

Expand E_a in the form

$$E_a(\theta) = -\frac{A_0}{\sin \theta} + \sum_{\nu_m} A_{\nu_m} \frac{\partial}{\partial \theta} T_{\nu_m}(\theta) \quad (19)$$

which is implied by (8b), where $\{A_{\nu_m}\}$ are unknown constants. Since $E_a(\theta)$ appears in both the numerator and the denominator of the right side of (18), normalize A_0 to unity. After carrying out the integrals in (18) using (19), Y_t becomes

$$\begin{aligned} Y_t = \frac{iZ_0}{2\pi Z_c^2} \left[-\sum_{s=1}^{\infty} \Omega(\psi_2) \frac{g_s^2(\mu_1, \mu_2)}{s(s+1)M_s I_{s,s}} \right. \\ + \sum_{\nu_m} \frac{\nu_m(\nu_m+1) \hat{I}_{\nu_m, \nu_m} A_{\nu_m}^2}{N_{\nu_m}} \\ - \sum_{s=1}^{\infty} \sum_{\nu_m} 2\Omega(\psi_2) \frac{g_s(\mu_1, \mu_2) I_{\nu_m, s} A_{\nu_m}}{M_s I_{s,s}} \\ \left. - \sum_{s=1}^{\infty} \sum_{\nu_m} \sum_{\nu_n} \Omega(\psi_2) \frac{s(s+1) I_{\nu_m, s} I_{\nu_n, s} A_{\nu_m} A_{\nu_n}}{M_s I_{s,s}} \right]. \end{aligned} \quad (20)$$

To simplify (20), introduce β_{ν_m} , α_{ν_m} , and γ_{ν_n, ν_m} as follows:

$$\beta_{\nu_m} = \frac{iZ_0}{2\pi Z_c^2} \nu_m(\nu_m+1) \frac{\hat{I}_{\nu_m, \nu_m}}{N_{\nu_m}}, \quad (21a)$$

$$\alpha_{\nu_m} = -\frac{iZ_0}{2\pi Z_c^2} \sum_{s=1}^{\infty} \Omega(\psi_2) g_s(\mu_1, \mu_2) \frac{I_{\nu_m, s}}{M_s I_{s,s}} \quad (21b)$$

$$\begin{aligned} \gamma_{\nu_n, \nu_m} &= \gamma_{\nu_m, \nu_n} \\ &= -\frac{iZ_0}{2\pi Z_c^2} \sum_{s=1}^{\infty} \Omega(\psi_2) s(s+1) \frac{I_{\nu_n, s} I_{\nu_m, s}}{M_s I_{s,s}}. \end{aligned} \quad (21c)$$

With (16) and (21), Y_t can be cast in the form

$$\begin{aligned} Y_t = Y_{t0} + \sum_{\nu_n} \beta_{\nu_n} A_{\nu_n}^2 + 2 \sum_{\nu_n} \alpha_{\nu_n} A_{\nu_n} \\ + \sum_{\nu_m} \sum_{\nu_n} \gamma_{\nu_m, \nu_n} A_{\nu_m} A_{\nu_n}. \end{aligned} \quad (22a)$$

Since Y_t is stationary with respect to the variation of E_a , one determines the unknown coefficients A_{ν_m} by setting $\frac{\partial}{\partial A_{\nu_m}} Y_t = 0$, which gives

$$\beta_{\nu_n} A_{\nu_n} + \alpha_{\nu_n} + \sum_{\nu_m} \gamma_{\nu_m, \nu_n} A_{\nu_m} = 0, \quad (22b)$$

Multiply (22b) by A_{ν_n} , sum over ν_n , and substitute the resulting expression into (22a) to obtain

$$Y_t = Y_{t0} + \sum_{\nu_n} \alpha_{\nu_n} A_{\nu_n}. \quad (23)$$

If the first term on the right side of (23) is called the *zero-order solution*, then the second expression may be called the *correction term*.

C. Wide-Angle Approximation

As stated earlier, in the wide-angle approximation, the complementary waves (TM modes) in the antenna region are negligible ($a_{\nu_p} \simeq 0$). This approximation corresponds to ψ_1 and ψ_2 that exceed 40° . Consequently, for $0 < r < a$ the field components can be expressed as

$$E_\theta = \frac{Z_0}{r \sin \theta} [\sigma_1 e^{-ikr} - \sigma_2 e^{ikr}]$$

and

$$H_\phi = \frac{1}{r \sin \theta} [\sigma_1 e^{-ikr} + \sigma_2 e^{ikr}] \quad (24)$$

where

$$\begin{aligned} \sigma_1 &= \frac{I_0}{2\pi} (Z_c Y_t + 1) e^{ika} \\ \sigma_2 &= \frac{I_0}{2\pi} (Z_c Y_t - 1) e^{-ika} \\ \frac{\sigma_2}{\sigma_1} &= \frac{Z_c Y_t - 1}{Z_c Y_t + 1} e^{-i2ka}. \end{aligned} \quad (25)$$

The ratio σ_2/σ_1 is the reflection coefficient.

In the exterior region ($r > a$)

$$E_\theta = iZ_0 \sum_{n=1}^{\infty} B_n \left[h_{n-1}^{(2)}(kr) - \frac{n}{kr} h_n^{(2)}(kr) \right] P_n^1(\cos \theta)$$

and

$$H_\phi = \sum_{n=1}^{\infty} B_n h_n^{(2)}(kr) P_n^1(\cos \theta) \quad (26)$$

where

$$h_n^{(2)}(x) = \sqrt{\frac{\pi}{2x}} H_{n+\frac{1}{2}}^{(2)}(x) \quad B_n = \frac{b_n}{2\pi a n(n+1) h_n^{(2)}(ka)} \quad (27a)$$

$$\begin{aligned} P_n^1(\cos \theta) &= -\frac{d}{d\theta} P_n(\cos \theta) = \sin \theta P_n'(\cos \theta) \\ &= \frac{n}{\sin \theta} [P_{n-1}(\cos \theta) - \cos \theta P_n(\cos \theta)]. \end{aligned} \quad (27b)$$

The prime in P_n' denotes differentiation with respect to its argument, and the function P_n^1 is the associated Legendre function. One can show that the input current $I(0)$ (which is not I_0) and the input voltage $V(0)$ are given by

$$\begin{aligned} I(0) &= \lim_{r \rightarrow 0} [2\pi r \sin \psi_1 H_\phi(r, \psi)] = 2\pi(\sigma_1 + \sigma_2) \\ V(0) &= \int_{\psi_1}^{\pi - \psi_2} r E_\theta(r, \theta) d\theta = 2\pi Z_c (\sigma_1 - \sigma_2). \end{aligned} \quad (28a)$$

Since

$$\begin{aligned} I_0 &= \pi(\sigma_1 e^{-ika} - \sigma_2 e^{ika}) \\ &= \frac{I(0)}{2[Z_c Y_t \cos(ka) + i \sin(ka)]} \end{aligned} \quad (28b)$$

clearly $I(0)$ is not necessarily equal I_0 . Moreover, the input impedance Z_{in} is given by

$$Z_{in} = \frac{V(0)}{I(0)} = Z_c \frac{\sigma_1 - \sigma_2}{\sigma_1 + \sigma_2}. \quad (29)$$

After setting $a_{\nu_p} = 0$ in (9) and using (27a), one determines that

$$B_n = -\frac{i}{2a} \frac{2n+1}{n(n+1)} \frac{(\sigma_1 e^{-ika} - \sigma_2 e^{ika}) g_n(\mu_1, \mu_2) \Omega(\psi_2)}{h_{n-1}^{(2)}(ka) - \frac{n}{ka} h_n^{(2)}(ka)}. \quad (30)$$

The substitution of B_n into (26) gives the field components in the exterior region ($r > a$). For observation points such that $kr \gg 1$, an asymptotic approximation of $h_n^{(2)}$ is

$$h_n^{(2)}(kr) \sim i^{n+1} \frac{e^{-ikr}}{kr}. \quad (31)$$

Hence, the radiated field

$$E_\theta^{\text{rad}}(r, \theta, \omega) = \frac{iZ_0}{2\pi} \frac{e^{-ikr}}{r} I(0) [kh_e(\theta, \omega)] \quad (32a)$$

is represented in terms of the antenna's effective height h_e , where

$$\begin{aligned} kh_e(\theta, \omega) &= \frac{e^{-ika} - \frac{\sigma_2}{\sigma_1} e^{ika}}{ka(1 + \frac{\sigma_2}{\sigma_1})} \sum_{n=1}^{\infty} \frac{i^{n-1} (2n+1)}{2n(n+1)} \\ &\quad \times \frac{P_n^1(\cos \theta) g_n(\mu_1, \mu_2) \Omega(\psi_2)}{h_{n-1}^{(2)}(ka) - \frac{n}{ka} h_n^{(2)}(ka)}. \end{aligned} \quad (32b)$$

Additional information is now used to derive an alternate representation for the coefficient preceding the summand in (32b) and to obtain Y_t under the wide-angle approximation. To these ends, equate the expressions in (24) and (26) at $r = a$ and use (2) and (30). After manipulation, one obtains the relation

$$\frac{1 + \frac{\sigma_2}{\sigma_1} e^{i2ka}}{1 - \frac{\sigma_2}{\sigma_1} e^{i2ka}} = -\frac{i\hat{S}}{4\pi(Z_c/Z_0)} = -iS \quad (33a)$$

where $S = \hat{S}Z_0/(4\pi Z_c)$

$$\begin{aligned} \hat{S} &= \sum_{n=1}^{\infty} \frac{2n+1}{n(n+1)} g_n^2(\mu_1, \mu_2) \zeta_n(ka) \Omega(\psi_2) \\ \zeta_n(ka) &= \frac{h_n^{(2)}(ka)}{h_{n-1}^{(2)}(ka) - \frac{n}{ka} h_n^{(2)}(ka)}. \end{aligned} \quad (33b)$$

Solving (33a) for σ_2/σ_1 leads to

$$\frac{\sigma_2}{\sigma_1} = e^{-i2ka} \frac{iS + 1}{iS - 1}. \quad (34a)$$

On comparing (25) and (34a), one arrives at

$$Y_t = -\frac{iS}{Z_c} = \frac{1}{Z_c} \frac{1 + \frac{\sigma_2}{\sigma_1} e^{i2ka}}{1 - \frac{\sigma_2}{\sigma_1} e^{i2ka}} \quad (34b)$$

for the terminal admittance.

Equations (32) and (34) provide expressions for the field, the effective height, and the terminal admittance under the wide-angle approximation. In the next two sections, these results are simplified for electrically small ($ka \ll 1$) and electrically large ($ka \gg 1$) wide-angle bicones.

1) *Small-Cone Approximation* ($ka \ll 1$): In this case, consider ζ_n of (33b) first. Through (27a), express ζ_n in terms of the Bessel functions of the first (J_ν) and second (Y_ν) kinds and substitute the standard asymptotic approximations of $J_\nu(ka)$ and $Y_\nu(ka)$ for the small argument ka [10]. In the resulting asymptotic approximation of ζ_n , one eliminates terms with $(ka)^n$ for $n \geq 2$ and expands the remaining expression in a series involving powers of (ka) with the binomial expansion. Finally, retaining only terms of the expansion through $(ka)^2$ inclusive leads to the approximation

$$\zeta_n(ka) \simeq -\frac{ka}{n} \left[1 + \frac{(ka)^2}{n(2n-1)} \right]. \quad (35a)$$

Next, substitute (35a) into (33b) to get

$$S \simeq -\frac{Z_0 ka}{4\pi Z_c} \sum_{n=1}^{\infty} \frac{2n+1}{n^2(n+1)} g_n^2(\mu_1, \mu_2) \Omega(\psi_2) + \mathcal{O}\left(\frac{(ka)^3}{2n^3}\right). \quad (35b)$$

Now an approximation of kh_e is obtained. One can argue that

$$\begin{aligned} h_{n-1}^{(2)}(ka) - \frac{n}{ka} h_n^{(2)}(ka) \\ \sim \frac{2^n \frac{(n-1)!}{(2n)!} i (ka)^{n+2}}{1 - \frac{x^2}{n(2n-1)} + i2^{2n} \frac{(n+1)!(n-1)!}{(2n+1)!(2n)!} (ka)^{2n+1}}. \end{aligned} \quad (36a)$$

Moreover, substituting (35b) into (34a) and expanding the trigonometric functions in Maclaurin series yield

$$\begin{aligned} \frac{e^{-ika} - \frac{\sigma_2}{\sigma_1} e^{ika}}{ka(1 + \frac{\sigma_2}{\sigma_1})} \\ \simeq -\frac{i}{(ka)^2} \left(\left[1 + \frac{Z_0 \Omega(\psi_2)}{4\pi Z_c(\psi_1, \psi_2)} \sum_{n=1}^{\infty} \frac{2n+1}{n^2(n+1)} g_n^2(\mu_1, \mu_2) \right] \right. \\ \left. - (ka)^2 \left[\frac{1}{6} + \frac{Z_0 \Omega(\psi_2)}{8\pi Z_c(\psi_1, \psi_2)} \sum_{n=1}^{\infty} \frac{2n+1}{n^2(n+1)} g_n^2(\mu_1, \mu_2) \right] \right. \\ \left. + \mathcal{O}((ka)^3) \right)^{-1}. \end{aligned} \quad (36b)$$

Substituting (36) into (32b) implies that

$$kh_e(\theta, \omega) \simeq \frac{N(\theta, \omega)}{D(\theta, \omega)} \quad (37a)$$

$$\begin{aligned} N(\theta, \omega) = -ka\Omega(\psi_2) \sum_{n=1}^{\infty} i^{n+1} 2^{n-1} \frac{(2n+1)(n-1)!}{n(n+1)(2n)!} \\ \times \frac{P_n^1(\cos \theta) g_n(\mu_1, \mu_2) (ka)^{n-1}}{1 - \frac{(ka)^2}{n(2n-1)} + i2^{2n} \frac{(n+1)!(n-1)!}{(2n+1)!(2n)!} (ka)^{2n+1}} \end{aligned} \quad (37b)$$

$$\begin{aligned} D(\theta, \omega) = \left[1 + \frac{Z_0 \Omega(\psi_2)}{4\pi Z_c(\psi_1, \psi_2)} \sum_{n=1}^{\infty} \frac{2n+1}{n^2(n+1)} g_n^2(\mu_1, \mu_2) \right] \\ - (ka)^2 \left[\frac{1}{6} + \frac{Z_0 \Omega(\psi_2)}{8\pi Z_c(\psi_1, \psi_2)} \right. \\ \left. \times \sum_{n=1}^{\infty} \frac{2n+1}{n^2(n+1)} g_n^2(\mu_1, \mu_2) \right] + \mathcal{O}((ka)^3). \end{aligned} \quad (37c)$$

By taking only the first term of each series and excluding terms of order $(ka)^2$ and higher, the approximations for S and kh_e can be simplified further to

$$S \simeq \frac{-3Z_0 \Omega(\psi_2)}{8\pi Z_c(\psi_1, \psi_2)} (\cos \psi_1 + \cos \psi_2)^2 ka \quad (38a)$$

$$kh_e \simeq \frac{6\pi Z_c(\psi_1, \psi_2) \Omega(\psi_2) (\cos \psi_1 + \cos \psi_2) \sin \theta}{8\pi Z_c(\psi_1, \psi_2) + 3Z_0 \Omega(\psi_2) (\cos \psi_1 + \cos \psi_2)^2} ka \quad (38b)$$

where $g_n^2(\mu_1, \mu_2) = \cos \psi_1 + \cos \psi_2$ and $P_1^1(\cos \theta) = \sin \theta$. The approximations in (38) are accurate provided ψ_2 is not near $\pi/2$ and $\psi_1 - \psi_2$ is not near zero; otherwise, more than one term in the series for S of (35b) is needed to obtain reasonable accuracy. For example, the second ($n = 2$) and third ($n = 3$) terms are not negligible compared to the first term ($n = 1$) for $\psi_1 = \psi_2$. According to (37) and (38b), the radiation pattern of an electrically small wide-angle bicone is approximately proportional to $\sin \theta$ and, consequently, is similar to the pattern of a short dipole, which agrees with an observation made in [8].

Another parameter of interest is the bicone's driving impedance Z_{in} of (29), which, by (34a) and (35b), is approximately (39a), shown at the bottom of the page, where the arguments of Z_c , Ω , and g_n are suppressed. Under the caveat on accuracy pertaining to (38a) and under the assumption that $(ka)^n$ is negligible for $n \geq 2$, a simpler approximation of Z_{in} is

$$\begin{aligned} Z_{in}(\psi_1, \psi_2) \\ \simeq \frac{8\pi Z_c^2(\psi_1, \psi_2)}{ika[8\pi Z_c(\psi_1, \psi_2) + 3Z_0 \Omega(\psi_2) (\cos \psi_1 + \cos \psi_2)^2]}. \end{aligned} \quad (39b)$$

As expected, the input impedance of an electrically small bicone behaves like a capacitive impedance $1/(i\omega C_{in})$, where the equivalent capacitance C_{in} is computed by making the obvious identification in either of (39).

An identity between two evaluations— $Y_{t0}(\psi_1, \psi_1)$ and $Y_{t0}(\psi_1, \pi/2)$ —of the zero-order approximation of the terminal admittance is now established. When either $\psi_2 = \pi/2$ or $\psi_2 = \psi_1$, the boundary conditions impose the constraint that

$$Z_{in} \simeq \frac{Z_c}{ika} \frac{1 - (ka)^2 \left[\frac{1}{2} + \frac{Z_0 \Omega}{4\pi Z_c} \sum_{n=1}^{\infty} \frac{2n+1}{n^2(n+1)} g_n^2 \right] + \mathcal{O}((ka)^4)}{\left[1 + \frac{Z_0 \Omega}{4\pi Z_c} \sum_{n=1}^{\infty} \frac{2n+1}{n^2(n+1)} g_n^2 \right] - \left[\frac{1}{6} + \frac{Z_0 \Omega}{8\pi Z_c} \sum_{n=1}^{\infty} \frac{2n+1}{n^2(n+1)} g_n^2 \right] (ka)^2 + \mathcal{O}((ka)^4)} \quad (39a)$$

the index r of the summation in (15) runs over the odd natural numbers only. Since $P_r(0) = 0$ for odd r

$$Y_{t0}(\psi_1, \psi_1) Z_c^2(\psi_1, \psi_1) = 2Y_{t0}(\psi_1, \pi/2) Z_c^2(\psi_1, \pi/2). \quad (40a)$$

However, $Z_c(\psi_1, \psi_1) = 2Z_c(\psi_1, \pi/2) = (Z_0/\pi) \ln[\cot(\psi_1/2)]$ by (2a), which implies that

$$Y_{t0}(\psi_1, \psi_1) = \frac{1}{2} Y_{t0}(\psi_1, \pi/2). \quad (40b)$$

Note that (40) and relations based on it do not depend on the small-cone approximation.

In summary, observe that the radiated field and the input impedance for the electrically small wide-angle bicone depend explicitly on the cone angles ψ_1 and ψ_2 . Moreover, upon setting $\psi_1 = \theta_0$, $\psi_2 = \pi/2$, and $\theta = \pi/2$, kh_e in (38b) and Z_{in} in (39b) reduce to

$$kh_e \simeq \frac{6\pi ka Z_c \cos \theta_0}{4\pi Z_c + 3Z_0 \cos^2 \theta_0} \quad (41)$$

and

$$Z_{in} \simeq \frac{4\pi Z_c^2}{ika(4\pi Z_c + 3Z_0 \cos^2 \theta_0)}$$

which are [9, Eq. (10)] and [11, Eq. (22)], respectively.

2) *Large-Cone Approximation* ($ka \gg 1$): In the high-frequency region, expressions for ζ_n and σ_2/σ_1 must be established to derive results for kh_e and Z_{in} . The analysis of this section extends the approach of [9, Appendixes B and C] to obtain the desired results for the more general situation of arbitrary ψ_1 and ψ_2 . In particular, an expression for σ_2/σ_1 is obtained by using identities involving the Legendre polynomials.

According to [12]

$$\sum_{l=1}^{\infty} \frac{2l+1}{l(l+1)} P_l(\mu_1) P_l(\mu_2) = 2 \ln 2 - 1 - \ln[(1-\mu_1)(1+\mu_2)] \quad (42a)$$

for $-1 < \mu_1 \leq \mu_2 < 1$ since $\mu_i \neq \pm 1$ and $\Omega(\psi_2) = 1$. Replacing μ_1 with $-\mu_1$ in (42a) and noting that $P_l(-\mu_1) = (-1)^l P_l(\mu_1)$ imply

$$\sum_{l=1}^{\infty} \frac{2l+1}{l(l+1)} (-1)^l P_l(\mu_1) P_l(\mu_2) = 2 \ln 2 - 1 - \ln[(1+\mu_1)(1+\mu_2)] \quad (42b)$$

for $-1 < -\mu_2 \leq \mu_1 < 1$. Set $\mu_2 = -\mu_1$ in (42b) to get

$$\sum_{l=1}^{\infty} \frac{2l+1}{l(l+1)} P_l^2(\mu_1) = 2 \ln 2 - 1 - \ln(1-\mu_1^2) \quad (42c)$$

for $-1 < \mu_1 < 1$. Consequently, by (2a), (7b), (42b), and

(42c), one obtains

$$\begin{aligned} \sum_{l=1}^{\infty} \frac{2l+1}{l(l+1)} g_l^2(\mu_1, \mu_2) &= \sum_{l=1}^{\infty} \frac{2l+1}{l(l+1)} [P_l^2(\mu_1) \\ &\quad - 2(-1)^l P_l(\mu_1) P_l(\mu_2) + P_l^2(\mu_2)] \\ &= 2 \ln \left[\cot \left(\frac{\psi_1}{2} \right) \cot \left(\frac{\psi_2}{2} \right) \right] \\ &= \frac{4\pi}{Z_0} Z_c(\psi_1, \psi_2) \end{aligned} \quad (43)$$

for $-1 < -\mu_1 \leq \mu_2 < 1$. Since $0 < \psi_i < \pi/2$ and $-\cos \psi_1 < \cos \psi_2$ for any ψ_1 and ψ_2 , the condition $-1 < -\mu_1 \leq \mu_2 < 1$ is satisfied. Hence, (43) is valid for the biconical geometry.

Before addressing σ_2/σ_1 , an asymptotic approximation for ζ_l is developed. By (31), one may argue for $l/(ka) < 1$ that

$$\begin{aligned} \zeta_l(ka) &\sim \frac{h_l^{(2)}(ka)}{h_{l-1}^{(2)}(ka) - \frac{l}{ka} h_l^{(2)}(ka)} \\ &\sim i \sum_{r=0}^{\infty} \left(\frac{li}{ka} \right)^r \sim i + \mathcal{O} \left(\frac{l}{ka} \right). \end{aligned} \quad (44a)$$

Thus, for fixed l

$$\lim_{ka \rightarrow \infty} \zeta_l(ka) = i. \quad (44b)$$

From (33b), (34a), and (44a), note that σ_2/σ_1 has two infinite sums where the index l runs from one to ∞ . Consequently, one may not simply substitute the asymptotic result for ζ_l into (34a) to get σ_2/σ_1 because l is not fixed. However, by taking advantage of the convergence of the two series

$$\sum_{l=1}^{\infty} \frac{2l+1}{l(l+1)} g_l^2(\mu_1, \mu_2) \zeta_l(ka) \quad \text{and} \quad \sum_{l=1}^{\infty} \frac{2l+1}{l(l+1)} g_l^2(\mu_1, \mu_2) \quad (45a)$$

and by using (44b), one may argue with mathematical rigor that

$$\begin{aligned} \lim_{ka \rightarrow \infty} \sum_{l=1}^{\infty} \frac{2l+1}{l(l+1)} g_l^2(\mu_1, \mu_2) \zeta_l(ka) \\ = i \sum_{l=1}^{\infty} \frac{2l+1}{l(l+1)} g_l^2(\mu_1, \mu_2) \\ = i \frac{4\pi}{Z_0} Z_c(\psi_1, \psi_2) \end{aligned} \quad (45b)$$

and

$$\lim_{ka \rightarrow \infty} \frac{iS+1}{iS-1} = 0 = \lim_{ka \rightarrow \infty} \frac{\sigma_2}{\sigma_1}. \quad (45c)$$

To determine the behavior of the effective length of the wide-angle bicone for $ka \gg 1$, one must evaluate two more summations involving the Legendre polynomials. First, let $\mu_2 = \mu = \cos \theta$ in (42a); second, interchange μ_1 and μ_2 in (42a) and let $\mu_2 = \mu$; third, let $\mu_1 = \mu$ in (42b); and fourth, interchange μ_1 and μ_2 in (42b), replace μ_1 with $-\mu_1$ and let

$\mu_1 = \mu$. Performing these manipulations leads to

$$\begin{aligned} & \sum_{l=1}^{\infty} \frac{2l+1}{l(l+1)} P_l(\mu) P_l(\mu_1) \\ &= \begin{cases} 2 \ln 2 - 1 - \ln[(1-\mu)(1+\mu_1)], & -1 < \mu \leq \mu_1 \\ 2 \ln 2 - 1 - \ln[(1-\mu_1)(1+\mu)], & \mu_1 \leq \mu < 1 \end{cases} \end{aligned} \quad (46a)$$

$$\begin{aligned} & \sum_{l=1}^{\infty} \frac{2l+1}{l(l+1)} (-1)^l P_l(\mu) P_l(\mu_2) \\ &= \begin{cases} 2 \ln 2 - 1 - \ln[(1-\mu_2)(1-\mu)], & -1 < \mu \leq -\mu_2 \\ 2 \ln 2 - 1 - \ln[(1+\mu)(1+\mu_2)], & -\mu_2 \leq \mu < 1. \end{cases} \end{aligned} \quad (46b)$$

After differentiating (46) with respect to μ , one obtains

$$\begin{aligned} & \sum_{l=1}^{\infty} \frac{2l+1}{l(l+1)} P_l^1(\mu) P_l(\mu_1) \\ &= \begin{cases} \sqrt{\frac{1+\mu}{1-\mu}}, & -1 < \mu \leq \mu_1 \\ -\sqrt{\frac{1-\mu}{1+\mu}}, & \mu_1 \leq \mu < 1 \end{cases} \end{aligned} \quad (47a)$$

$$\begin{aligned} & \sum_{l=1}^{\infty} \frac{2l+1}{l(l+1)} (-1)^l P_l^1(\mu) P_l(\mu_2) \\ &= \begin{cases} \sqrt{\frac{1+\mu}{1-\mu}}, & -1 < \mu \leq -\mu_2 \\ -\sqrt{\frac{1-\mu}{1+\mu}}, & -\mu_2 \leq \mu < 1. \end{cases} \end{aligned} \quad (47b)$$

The last ingredient necessary for calculating the limit of kh_e is the asymptotic result

$$h_{l-1}^{(2)}(ka) - \frac{l}{ka} h_l^{(2)}(ka) \sim \frac{i^l}{ka} e^{-ika} \left[1 - \frac{li}{ka} \right] \quad (48)$$

as $ka \rightarrow \infty$. Equation (48) implies

$$\begin{aligned} & \lim_{ka \rightarrow \infty} \sum_{l=1}^{\infty} \frac{2l+1}{l(l+1)} \frac{i^{l-1} e^{-ika} P_l^1(\mu) g_l(\mu_1, \mu_2)}{ka [h_{l-1}^{(2)}(ka) - \frac{l}{ka} h_l^{(2)}(ka)]} \\ &= -i \sum_{l=1}^{\infty} \frac{2l+1}{l(l+1)} P_l^1(\mu) g_l(\mu_1, \mu_2). \end{aligned} \quad (49)$$

Substituting (45d) and (49) into (32b) and using (47) yield

$$\begin{aligned} & \lim_{ka \rightarrow \infty} kh_e(\theta, \omega) \\ &= \lim_{ka \rightarrow \infty} \frac{1 - \frac{\sigma_2}{\sigma_1} e^{i2ka}}{1 + \frac{\sigma_2}{\sigma_1}} \frac{\Omega(\psi_2)}{2} \\ &\quad \times \sum_{l=1}^{\infty} \frac{2l+1}{l(l+1)} \frac{i^{l-1} e^{-ika} P_l^1(\mu) g_l(\mu_1, \mu_2)}{ka [h_{l-1}^{(2)}(ka) - \frac{l}{ka} h_l^{(2)}(ka)]} \\ &= -\frac{i}{2} \Omega(\psi_2) \sum_{l=1}^{\infty} \frac{2l+1}{l(l+1)} P_l^1(\mu) [P_l(\mu_1) - (-1)^l P_l(\mu_2)] \\ &= -\frac{i}{2} \Omega(\psi_2) \\ &\quad \times \begin{cases} 0, & -1 < \mu \leq -\mu_2 \text{ or } \mu_1 \leq \mu < 1 \\ \sqrt{\frac{1+\mu}{1-\mu}} + \sqrt{\frac{1-\mu}{1+\mu}}, & -\mu_2 < \mu < \mu_1 \end{cases} \\ &= -i \Omega(\psi_2) \begin{cases} 0, & \theta \text{ in } (0, \psi_1) \text{ or } [\pi - \psi_2, \pi] \\ 1/\sin \theta, & \theta \text{ in } (\psi_1, \pi - \psi_2). \end{cases} \end{aligned} \quad (50)$$

TABLE I
CORRESPONDENCE AMONG UPPER LIMIT M OF APPROXIMATE RADIATION
DISTRIBUTION FUNCTION R_M , ka , AND FREQUENCY f IN FIG. 3.

Figure	f	ka	Range of ka	M Used	M Needed
3a	1 MHz	0.0106	$ka \ll 1$	29	3
3b	100 MHz	1.0640	Transitional	29	3
3c	500 MHz	5.3198	Transitional	29	3
3d	1 GHz	10.6395	Transitional	29	6
3e	10 GHz	106.3950	$ka \gg 1$	60	60
3f	10 GHz	106.3950	$ka \gg 1$	29	60

This limit implies that the behavior of the field $|E_\theta|$ for $\psi_1 < \theta < \pi - \psi_2$ approaches $1/\sin \theta$ as the frequency increases without bound and that the directions of maximum radiation approach ψ_1 and $\pi - \psi_2$. Consequently, maximum radiation of the electrically large wide-angle bicone does not occur at broadside ($\theta = \pi/2$).

Furthermore, with (29) and (45c), one can easily show that the bicone's input impedance has the limit

$$\lim_{ka \rightarrow \infty} Z_{\text{in}} = Z_c(\psi_1, \psi_2). \quad (51)$$

Thus, for high frequencies the input impedance is essentially constant. Hence, the electrically large wide-angle bicone is a broadband and possibly an ultrawide-band antenna.

3) *Examples:* Two special cases are considered for $a = 20$ in: 1) $\psi_1 = 53.1^\circ = \psi_2$ and 2) $\psi_1 = 53.1^\circ$ and $\psi_2 = 70^\circ$. The relative field pattern associated with the E -plane radiation pattern [7]

$$\begin{aligned} R(\theta, \omega) &= \frac{E_\theta^{\text{rad}}(r, \theta, \omega)}{E_\theta^{\text{rad}}(r, \pi/2, \omega)} \\ &= \frac{\sum_{n=1}^{\infty} \frac{i^{n-1} (2n+1)}{2n(n+1)} \frac{P_n^1(\cos \theta) g_n(\mu_1, \mu_2)}{h_{n-1}^{(2)}(ka) - \frac{n}{ka} h_n^{(2)}(ka)}}{\sum_{n=1}^{\infty} \frac{i^{n-1} (2n+1)}{2n(n+1)} \frac{P_n^1(0) g_n(\mu_1, \mu_2)}{h_{n-1}^{(2)}(ka) - \frac{n}{ka} h_n^{(2)}(ka)}} \end{aligned} \quad (52)$$

is plotted for various values of ka in both cases.

In case 1), as mentioned previously, only the odd terms of the series are present because $\psi_1 = \psi_2$. Hence, on re-indexing each sum in (52) by setting $n = 2m + 1$ and by allowing m to run from zero to ∞ , (52) becomes [8, Eq. (6)]. Truncate each series of the re-indexed version of (52) at $M + 1$ terms and denote the resulting fraction as R_M . The approximate pattern $|R_M|$ is plotted in Fig. 3 for five frequencies ranging from $ka \ll 1$ to $ka \gg 1$. The correspondence between ka and frequency f for each plot is shown in Table I. One high frequency and one low frequency are chosen to represent situations when $ka \gg 1$ and $ka \ll 1$, respectively; while the other three frequencies are selected for comparison to [8, Fig. 5(c)], as well as for providing nominal values in the transition between $ka \ll 1$ and $ka \gg 1$. The pattern $|R_M|$ has azimuthal symmetry and symmetry about $\theta = \pi/2$. The former means that the pattern may be graphed in two dimensions and the latter means that one may restrict θ to $[0, \pi/2]$ to gain a complete understanding of the behavior of $|R|$.

As one can observe [Fig. 3(a)], the pattern at low frequencies is similar to that of the short dipole as [8] notes. In fact, on utilizing the low-frequency approximation in (38b), one finds that $R \sim \sin \theta$, which is the short-dipole pattern. The graph of $R \sim \sin \theta$ is coincident with that of Fig. 3(a) when they are

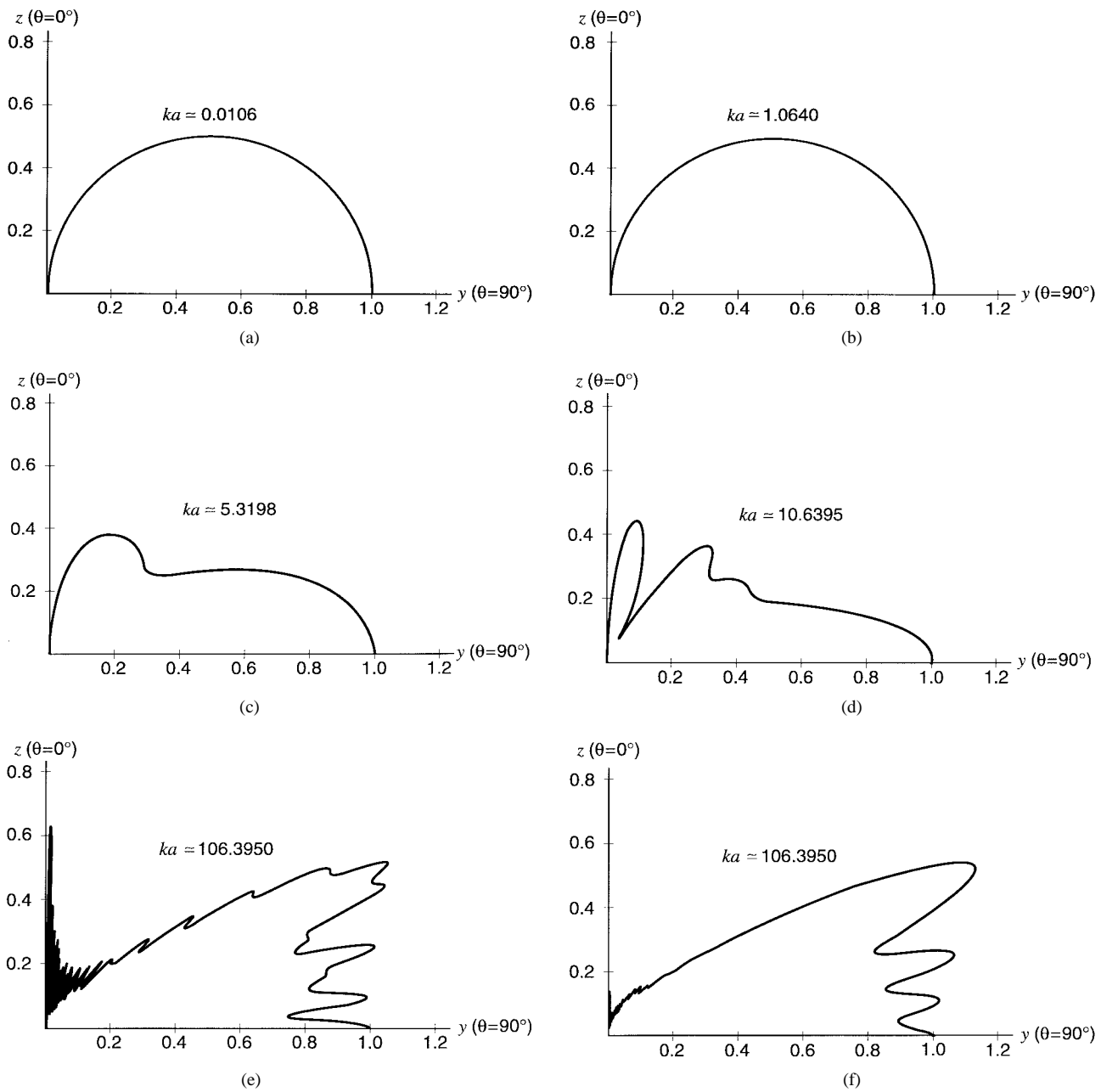


Fig. 3. Approximate magnitude $|R_M|$ of the normalized radiation distribution of E_θ (E -plane radiation pattern) for a spherically capped biconical antenna with equal cone angles in free space. The cone angles ψ_1 and ψ_2 are equal to 53.1° , and the slant height (height) is 20 in (12 in). (a) $ka = 0.0106$. (b) 1.0640. (c) 5.3198. (d) 10.6395. (e) 106.3950. (f) $|R_M|$ is graphed less accurately for $ka = 106.3950$ by using only 30 terms ($M = 29$) of each series in (52).

overlaid. Even the pattern for the transitional value of $ka = 1.0640$ is only slightly distinguishable from the short dipole's pattern. Therefore, the approximation for $ka \ll 1$ is excellent for $ka \leq 0.2$ and is good for $0.2 < ka \leq 1.06$. As ka increases from 1 to 10.640 through the transitional region between electrically small and electrically large bicones [Fig. 3(b)–(d)], the peak radiation remains at broadside; however, the radiation decreases for $18^\circ \leq \theta < 90^\circ$, and for each θ between 0° and 18° the radiation level exceeds that of the short dipole with a local maximum appearing at some intermediate angle. Fig. 3(b)–(d) agrees well with [8, Fig. 5(c)]. Sandler and King don't indicate how many terms of the series they use to generate their figures; however in the *Mathematica* calculations used to generate Fig. 3, one obtains good graphical depictions for

$ka = 1.0640, 5.3198, 10.6395$ when $M = 3, 3, 6$, respectively. As Table I indicates, Fig. 3(a)–(d) is generated for 30 terms of each series ($M = 29$). This value of M is picked because each pattern is accurate for $ka \leq 10.6395$ and because Harrison used this value for calculating tables in [11].

In contrast, to obtain a reasonably accurate pattern for $ka = 106.3950$, at least 61 terms ($M = 60$) must be used [Fig. 3(e)]. Fig. 3(f) plots $ka = 106.3950$ for 30 terms and is provided as a comparison to Fig. 3(e). Clearly, the detail is missing in Fig. 3(f). The pattern in Fig. 3(e) is considerably less smooth than the patterns for small and transitional values of ka . In particular, many smaller amplitude lobes appear for $0^\circ < \theta \leq 30^\circ$. The effect is less pronounced between 30° and 90° , where the pattern has a somewhat wavy nature as

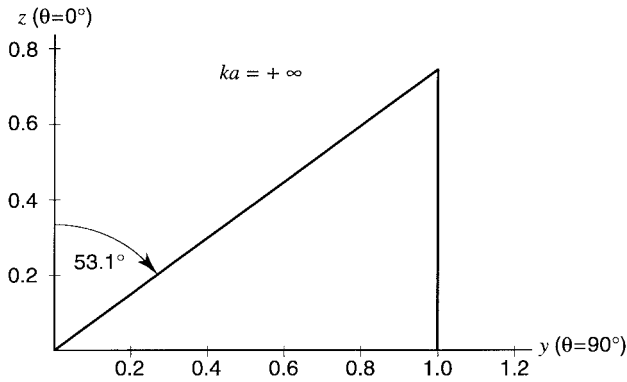


Fig. 4. E -plane radiation pattern in the high-frequency limit ($ka \rightarrow +\infty$) for a spherically capped biconical antenna with equal cone angles in free space. The cone angles ψ_1 and ψ_2 are equal to 53.1° and the slant height (height) is 20 in (12 in).

evidenced by the five local maxima and four local minima. The lobe structure for small θ is not unexpected because the number of oscillations and the magnitude near $\theta = 0$ of the Associated Legendre Function $P_{2m+1}^1(\cos\theta)$ increase as m increases. Consequently, as ka increases, M must increase to get accurate results. One major feature that distinguishes the pattern of a wide-angle bicone for high frequencies from the patterns at other frequencies is the migration of the direction of peak radiation away from broadside. In Fig. 3(e), the peak occurs well off broadside at $\theta = 63.5^\circ$. As ka increases, one expects the peak to approach the cone's surface at $\psi_1 = 53.1^\circ$ since by (50) and (52), $R(\theta, \omega) \rightarrow 1/\sin\theta$ as $ka \rightarrow \infty$ for $\psi_1 < \theta \leq \pi/2$. The limiting value in Fig. 4 is the triangular region bounded by $R = 1/\sin\theta$ (the vertical line segment $y = 1$), the line $z = 0$, and the line $z = y \cot(53.1^\circ)$. Consequently, as $ka \rightarrow \infty$, the pattern calculated with (52) will approach the pattern of Fig. 4. Fig. 3(e) is consistent with Fig. 4 in that most of the energy is radiated in $50^\circ \leq \theta \leq 90^\circ$ and the five local maxima are very close to the vertical line $y = 1$.

In case 2), the summations in (52) are truncated at N terms and the resulting fraction is denoted R_N . Although not shown, the pattern looks like that of the short dipole for $ka \leq 1$. As ka increases from unity through transitional values, the effect of distinct bicone angles is manifested in asymmetrical patterns relative to the y axis. Specifically, in the limit as $ka \rightarrow +\infty$, $|R_N| \rightarrow 1/\sin\theta$. Moreover, the pattern approaches the triangular region bounded by the lines $R = 1/\sin\theta$, $z = -y \cot(70^\circ)$, and $z = y \cot(53.1^\circ)$, which are indicated by the dashed line segments in Fig. 5. To illustrate the behavior for large ka , Fig. 5 also displays the pattern for $ka = 106.3950$ and $N = 120$ (solid curve). This pattern has many small amplitude lobes for $0^\circ \leq \theta \leq 50^\circ$ and $110^\circ \leq \theta \leq 180^\circ$. For angles between 60° and 108° , several relative maxima and minima occur near the line $y = 1$, with the two largest maxima at $\theta = 63.8^\circ$ and 99.7° . As ka and N increase, the number of these local extrema increases and the associated $|R_N|$ approaches the line $y = 1$ with the largest and second largest values of $|R_N|$ approaching the edges of the upper and lower cones, respectively. The two obvious differences from case 1) are: a) the loss of symmetry in the

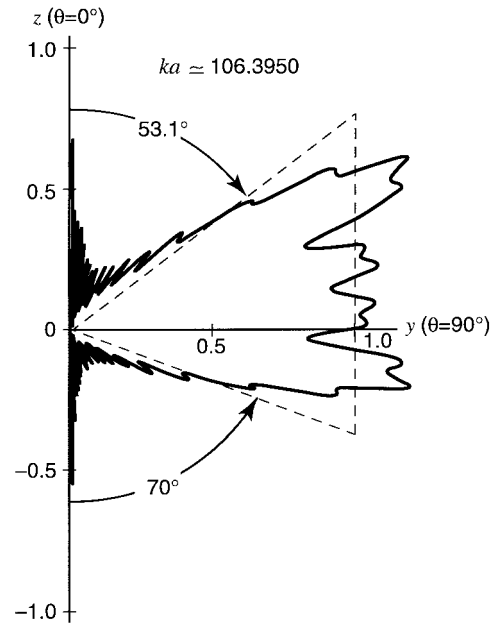


Fig. 5. Approximate pattern with $ka = 106.3950$ and $N = 120$ (solid curve) and high-frequency limit pattern (dashed curves) for a spherically capped biconical antenna with unequal cone angles in free space. The cone angles ψ_1 and ψ_2 are 53.1° and 70° , respectively, and the slant height (height) is 20 in (12 in).

pattern about the y axis of case 2) and b) the peak radiation occurs near the cone with the smaller cone angle in case 2).

These examples provide analytical justification of Sandler and King's numerically based observations [8] that the wide-angle bicone behaves like a short dipole at low frequencies (38b) and has its direction of maximum radiation moving away from broadside toward the bicone's surface for high frequencies (50). Consequently, the tacit assumption in [9, Appendixes B and C] that the peak radiation occurs at $\theta = \pi/2$ for electrically large bicones is not justified. Since an ultrawide-band input signal's passband [13] may contain both low- and high-frequency spectral components relative to the bicone's passband, the explicit analytical characterizations of the frequency-dependent behavior contained herein are essential in analyzing radiation of ultrawide-band signals.

III. TIME HISTORY OF RADIATED AND RECEIVED FIELDS ASSOCIATED WITH ELECTRICALLY SMALL AND ELECTRICALLY LARGE WIDE-ANGLE BICONES

Thus far, the discussion of electrically small and large wide-angle conical antennas has concentrated on the impact to quantities in the frequency domain. Of interest, especially when the input is wide-band or ultrawide-band, is the temporal behavior of the radiated field and received voltage. This section expresses the time-domain radiated field of wide-angle conical antennas in terms of the input voltage and expresses the time-dependent load voltage of a receiving conical antenna in terms of the incident field. In particular, four special cases are considered: 1) transmission for $ka \ll 1$; 2) transmission for $ka \gg 1$; 3) reception for $ka \ll 1$; and 4) reception for $ka \gg 1$.

Let $V_g(t)$ be the input source voltage of the transmitting antenna, and let $\hat{V}_g(\omega)$ be the Fourier transform of $V_g(t)$. If $Z_{\text{in}}(\omega)$ and $Z_g(\omega)$ are the input impedance of the antenna and the generator (source) impedance, respectively, the input current $I(0)$ (or $I(0, \omega)$) and $\hat{V}_g(\omega)$ are related by

$$I(0) = \frac{\hat{V}_g(\omega)}{Z_{\text{in}}(\omega) + Z_g(\omega)}. \quad (53)$$

Substituting (53) into (32a) yields

$$E_{\theta}^{\text{rad}}(r, \theta, \omega) = \frac{iZ_0}{2\pi} \left[\frac{\hat{V}_g(\omega)}{Z_{\text{in}}(\omega) + Z_g(\omega)} \right] \frac{e^{-ikr}}{r} kh_e(\theta, \omega). \quad (54)$$

Consequently, the transfer function $T(r, \theta, \omega)$ of the transmitting antenna is defined by

$$\begin{aligned} T(r, \theta, \omega) &= \frac{E_{\theta}^{\text{rad}}(r, \theta, \omega)}{\hat{V}_g(\omega)} \\ &= \frac{i\omega Z_0}{cr} \frac{h_e(\theta, \omega) e^{-i\omega r/c}}{Z_{\text{in}}(\omega) + Z_g(\omega)}. \end{aligned} \quad (55)$$

The time-dependent radiated field $e_{\theta}^{\text{rad}}(r, \theta, t)$, the inverse Fourier transform of $E_{\theta}^{\text{rad}}(r, \theta, \omega)$, is given formally by

$$\begin{aligned} e_{\theta}^{\text{rad}}(r, \theta, t) &= \frac{1}{2\pi} \int_{-\infty}^{\infty} E_{\theta}^{\text{rad}}(r, \theta, \omega) e^{i\omega t} d\omega \\ &= \frac{1}{2\pi} \int_{-\infty}^{\infty} \hat{V}_g(\omega) T(r, \theta, \omega) e^{i\omega t} d\omega. \end{aligned} \quad (56)$$

When the antenna is receiving, define the open-circuit receiving voltage $\hat{V}_{\text{oc}}(\omega)$ by

$$\hat{V}_{\text{oc}}(\omega) = -E_{\theta}^{\text{inc}}(r, \theta, \omega) h_e(\theta, \omega). \quad (57a)$$

In this expression, θ gives the direction of the incident field relative to the axis of the receiving bicone. If the receiving antenna is connected to a load with impedance $Z_L(\omega)$, then the received voltage \hat{V}_L across this load is

$$\hat{V}_L(\omega) = \frac{E_{\theta}^{\text{inc}}(r, \theta, \omega) h_e(\theta, \omega) Z_L(\omega)}{Z_{\text{in}}(\omega) + Z_L(\omega)} \quad (57b)$$

where Z_{in} is the input impedance of the antenna and is the same impedance when the antenna is used for transmitting. One can also define the reception transfer function $S(\theta, \omega)$ by

$$S(\theta, \omega) = \frac{\hat{V}_L(\omega)}{E_{\theta}^{\text{inc}}(r, \theta, \omega)} = -\frac{h_e(\theta, \omega) Z_L(\omega)}{Z_{\text{in}}(\omega) + Z_L(\omega)}. \quad (57c)$$

Therefore, the time-dependent load voltage V_L is given formally by

$$\begin{aligned} V_L(t) &= \frac{1}{2\pi} \int_{-\infty}^{\infty} \frac{\hat{V}_{\text{oc}}(\omega) Z_L(\omega) e^{i\omega t}}{Z_{\text{in}}(\omega) + Z_L(\omega)} d\omega \\ &= \frac{1}{2\pi} \int_{-\infty}^{\infty} E_{\theta}^{\text{inc}}(r, \theta, \omega) S(\theta, \omega) e^{i\omega t} d\omega. \end{aligned} \quad (58)$$

When $\hat{V}_g(\omega)$ and $E_{\theta}^{\text{inc}}(r, \theta, \omega)$ are known, $e_{\theta}^{\text{rad}}(r, \theta, t)$ and $V_L(t)$ can be expressed in closed form either for $ka \ll 1$ or for $ka \gg 1$ under suitable matching conditions. Harrison and Williams [9] considered transient radiation from and reception by wide-angle conical antennas above an infinite conducting plane for various special cases when the observation angle θ is $\pi/2$. Instead of presenting all the cases enumerated in [9], a few cases are presented for illustrative purposes.

Case 1: Consider radiation from a wide-angle electrically small bicone which is matched to the source ($Z_c = Z_g$). Substituting (39b) for Z_{in} and (38b) for kh_e in (54) and (56) yields

$$\begin{aligned} e_{\theta}^{\text{rad}}(r, \theta, t) &= \frac{3\Omega(\psi_2) Z_0 a^2 (\cos \psi_1 + \cos \psi_2)}{8\pi^2 c^2 r Z_c(\psi_1, \psi_2)} \\ &\quad \times \sin \theta \frac{d^2}{dt^2} V_g\left(t - \frac{r}{c}\right) \end{aligned} \quad (59)$$

where $|-8i\pi Z_c| \gg ka[8\pi Z_c + 3Z_0\Omega(\cos \psi_1 + \cos \psi_2)^2]$ is satisfied for $ka \ll 1$. Equation (59) shows that for a wide-angle small cone the radiated electric field is proportional to the second time derivative of the retarded input voltage, provided the matching condition $Z_c = Z_g$ is also satisfied. This result is similar to that of a short dipole, which has a spatially invariant current.

Case 2: As a second example, assume the matching condition of Case 1, but let the antenna be electrically large. Equations (50), (51), and (56) lead to

$$e_{\theta}^{\text{rad}}(r, \theta, t) = \frac{Z_0}{4\pi r Z_c(\psi_1, \psi_2) \sin \theta} V_g\left(t - \frac{r}{c}\right). \quad (60)$$

Thus, for a large wide-angle conical radiator, the field is a retarded replica of the input voltage and is maximized along the conic surface corresponding to the smaller of the two cone angles where the $\sin \theta$ is a minimum. Consequently, this antenna is ideal for ultrawide-band signals with spectra that obey the constraint $ka \gg 1$.

Case 3: In this case, the voltage received by a small bicone that is matched to its load ($Z_L = Z_c$) is obtained. After substituting (39a) for Z_{in} and (38b) for kh_e in (58), one gets

$$\begin{aligned} V_L(t) &= -\frac{3a^2}{4c} \Omega(\psi_2) (\cos \psi_1 + \cos \psi_2) \\ &\quad \times \sin \theta \left[\frac{1}{2\pi} \int_{-\infty}^{\infty} i\omega E^{\text{inc}}(r, \theta, \omega) e^{i\omega t} d\omega \right] \\ &= -\frac{3a^2}{4c} \Omega(\psi_2) (\cos \psi_1 + \cos \psi_2) \sin \theta \frac{d}{dt} e_{\theta}^{\text{inc}}(r, \theta, t). \end{aligned} \quad (61)$$

Hence, the received voltage for a small wide-angle bicone under ideal matching conditions behaves like the temporal derivative of the incident field.

Case 4: Finally, reception by an electrically large wide-angle bicone with a matched load ($Z_L = Z_c$) is considered. Equations (50), (51), and (58) imply

$$\begin{aligned} V_L(t) &= -\frac{c}{2\sin \theta} \left[\frac{1}{2\pi} \int_{-\infty}^{\infty} \frac{1}{i\omega} E^{\text{inc}}(r, \theta, \omega) e^{i\omega t} d\omega \right] \\ &= -\frac{c}{2\sin \theta} \int_{-\infty}^t e_{\theta}^{\text{inc}}(r, \theta, \tau) d\tau. \end{aligned} \quad (62)$$

Clearly, in the preceding cases, the time-dependent radiated field and received load voltage are functions of the input signal's passband and the matching condition between the antenna and the input's passband. Cases 1 and 2 indicate that under perfect matching conditions the radiated field has different temporal dependences, as well as the previously stated $\sin \theta$ and $1/\sin \theta$ dependences, for $ka \ll 1$ and $ka \gg 1$; that is, the field is proportional to the second time derivative of the retarded input voltage and to the retarded input voltage for $ka \ll 1$ and $ka \gg 1$, respectively. On the other hand, the received load voltage is proportional to the product of $\sin \theta$ ($1/\sin \theta$) and the time derivative (integral) of the incident field for $ka \ll 1$ ($ka \gg 1$). Furthermore, variations of ψ_1 and ψ_2 affect only the amplitudes of the radiated field and received voltage for these cases.

IV. SUMMARY

The results of this study are valid for spherically capped wide-angle biconical antenna configurations, including the degenerate cases of a cone above a ground plane and a bicone with equal cone angles ($\psi_1 = \psi_2$). In addition, the treatment for arbitrary cone angles ψ_1 and ψ_2 subsumes as special cases the results of [1]–[9], [11]. In particular, to the best of the authors' knowledge, the results for unequal conical angles are new. Exact and approximate expressions for the driving impedance, the effective height, and the radiated field are derived in the frequency domain. Moreover, the approximate expressions derived herein for electrically small ($ka \ll 1$) and large ($ka \gg 1$) bicones are more accurate than the corresponding ones in the literature. Also, time-domain representations of the radiated field and the received load voltage for $ka \ll 1$ and $ka \gg 1$ have been derived under different matching conditions. The radiated field and the received voltage vary like $\sin \theta$ for small wide-angle bicones and like $1/\sin \theta$ for large wide-angle bicones.

Sandler and King's observations regarding the behavior of electrically small (low frequencies) and electrically large (high frequencies) wide-angle bicones are explained by the analytical work of this paper. Furthermore, since the results of Sandler and King (as well as the authors' results) show that maximum radiation does not take place at broadside ($\theta = \pi/2$) for high frequencies, consideration only of the broadside case by Harrison and Williams [9] for $ka \gg 1$ is inadequate. In particular, the authors show that maximum radiation occurs along the cone with smaller cone angle. The results contained herein are especially pertinent to ultrawide-band signals, since the passband of such signals may include low, transitional, and high frequencies of a wide-angle bicone's passband.

Finally, while reproducing some of the numerical results of Sandler and King, a new piece of information has been discovered. Namely, the infinite series for the radiated far field is very slowly convergent for certain high frequencies, which may correspond to the electrical resonances of the conical structure. This aspect of biconical radiation problems requires further detailed investigation.

ACKNOWLEDGMENT

The authors thank S. K. Guilmineau for help with the figures.

REFERENCES

- [1] S. A. Schelkunoff, *Electromagnetic Waves*. New York: Van Nostrand, 1943, ch. XI.
- [2] P. D. P. Smith, "The conical dipole of wide-angle," *J. Appl. Phys.*, vol. 19, pp. 11–23, 1948.
- [3] C. T. Tai, "On the theory of biconical antennas," *J. Appl. Phys.*, vol. 19, pp. 1155–1160, 1948.
- [4] ———, "A study of the E.M.F. method," *J. Appl. Phys.*, vol. 20, pp. 717–723, 1949.
- [5] ———, "Application of variational principle to biconical antennas," *J. Appl. Phys.*, vol. 20, pp. 1076–1084, 1949.
- [6] C. H. Papas and R. W. P. King, "Input impedance of wide-angle conical antennas fed by a coaxial line," *Proc. IRE*, vol. 37, pp. 1269–1271, 1949.
- [7] ———, "Radiation from wide-angle conical antennas fed by a coaxial line," *Proc. IRE*, vol. 39, pp. 49–51, 1951.
- [8] S. S. Sandler and R. W. P. King, "Compact conical antennas for wide-band coverage," *IEEE Trans. Antennas Propagat.*, vol. 42, pp. 436–439, Mar. 1994.
- [9] C. W. Harrison and C. S. Williams, "Transients in wide-angle conical antennas," *IEEE Trans. Antennas Propagat.*, vol. AP-13, pp. 230–246, Mar. 1965.
- [10] F. W. J. Olver, "Bessel functions of integer order," in *Handbook of Mathematical Functions with Formulas, Graphs, and Mathematical Tables*, M. Abramowitz and I. A. Stegun, Eds. New York: Dover, 1965, p. 360.
- [11] C. W. Harrison Jr., "Tables of impedance and radian effective length of wide-angle conical antennas," Sandia Nat. Labs., Albuquerque, NM, Rep. SC-R-662, June 1963.
- [12] A. Erdelyi, *Higher Transcendental Functions*. New York: McGraw-Hill, 1953, vol. 2, p. 183 [Eq. (53)] (Bateman manuscript project).
- [13] J. G. Siambis and R. E. Symons, "Ultrawide-band clustered-cavity™ klystron," in *Ultra-Wideband, Short-Pulse Electromagnetics*, H. L. Bertoni, L. Carin, and L. B. Felsen, Eds. New York: Plenum, 1993, p. 121.



Surendra N. Samaddar (S'58–M'62–SM'68–LS'93) was born in Bengal, India. He received the B.Sc. degree in mathematics and the M.Sc. degree in applied physics from the University of Calcutta, India, in 1948 and 1950, respectively, and the Ph.D. degree from the University of Michigan at Ann Arbor in electrical engineering, in 1962.

From 1951 to 1952, he received training in telecommunication engineering from the Indian Post & Telegraph Department, Calcutta. From 1953 to 1957 he was employed by M/S Ericsson Telephone Company, Calcutta, as an Engineer. From 1957 to 1959 he worked at the Microwave Research Institute of the Polytechnic Institute, Brooklyn, NY, as a Senior Research Fellow while pursuing graduate studies in electrical engineering. He joined the Raytheon Company, Wayland and Sudbury, MA, in 1962 as a Senior Scientist and was responsible for conducting theoretical research in radiation from antennas, in propagation through various media including plasmas, and in scattering from reentry bodies. He joined Calspan Corporation (formerly Cornell Laboratories), Buffalo, NY, in 1970 and worked in sound-wave propagation in oceanic waters, wave propagation in random media, and scattering from turbulent wakes behind bodies reentering the Earth's atmosphere. In 1974 he joined GTE Sylvania, Boston, MA, where he worked on EMP, ELF, VLF, and UHF propagation. From 1976 to 1982 he was with the Research and Development Office of the U.S. Coast Guard, Washington, DC, specializing in Loran-C signal propagation studies. Since October 1982, he has been with the Radar Division of the Naval Research Laboratory (NRL), Washington, DC. He has published over 60 journal articles. His research interests include antenna theory, electromagnetic wave propagation near the Earth's surface, pulsed radiation from antennas, enhancement of the Fresnel near-field region of a radiator by pulsed excitations, and pulse propagation in a dispersive medium.



Eric L. Mokole (M'86) was born in Akron, OH, in 1949. He received the B.S. degree in applied mathematics from New York University, NY, in 1971, the M.S. degree in mathematics from Northern Illinois University, DeKalb, in 1973, the M.S. degrees in physics and applied mathematics from the Georgia Institute of Technology, Atlanta, in 1976 and 1978, respectively, and the Ph.D. degree in mathematics from the Georgia Institute of Technology, in 1982.

For the 1982–1983 academic year, he was an Assistant Professor of Mathematics at Kennesaw College, Kennesaw, GA. From 1983 to 1986 he held a position in the Electronic Warfare Division of the Naval Intelligence Support Center (now the Office of Naval Intelligence), Washington, DC. Since 1986 he has been employed by the Radar Division of the Naval Research Laboratory (NRL), Washington, DC. Currently, he is a member of the consulting staff of the Target Characteristics Branch. He has been conducting basic/applied research and system analyses on space-based radar, on shipborne Navy radars and the associated electronic countermeasures (ECM) and electronic counter-countermeasures (ECCM), as well as on ultrawide-band radar. These efforts have involved signal processing, non-Gaussian detection theory, data analysis, system simulation/modeling, threat/ECM modeling, information extraction, and ionospheric/low-altitude/ultrawide-band electromagnetics.

Dr. Mokole is a member of the American Geophysical Union, the American Mathematical Society, the American Physical Society, IEEE Societies on Aerospace and Electronic Systems, Antennas and Propagation, and Geoscience and Remote Sensing, Sigma Xi, and the Society for Industrial and Applied Mathematics.